



CHORUS

This is the accepted manuscript made available via CHORUS. The article has been published as:

Nanophotonic Quantum Storage at Telecommunication Wavelength

Ioana Craiciu, Mi Lei, Jake Rochman, Jonathan M. Kindem, John G. Bartholomew, Evan Miyazono, Tian Zhong, Neil Sinclair, and Andrei Faraon

Phys. Rev. Applied **12**, 024062 — Published 30 August 2019

DOI: [10.1103/PhysRevApplied.12.024062](https://doi.org/10.1103/PhysRevApplied.12.024062)

Nanophotonic quantum storage at telecommunication wavelength

Ioana Craiciu,^{1,2} Mi Lei,^{1,2} Jake Rochman,^{1,2} Jonathan M. Kindem,^{1,2} John G. Bartholomew,^{1,2}
Evan Miyazono,^{1,2} Tian Zhong,^{1,2,*} Neil Sinclair,^{3,4} and Andrei Faraon^{1,2,†}

¹*Kavli Nanoscience Institute and Thomas J. Watson, Sr., Laboratory of Applied Physics,
California Institute of Technology, Pasadena, California 91125, USA*

²*Institute for Quantum Information and Matter,
California Institute of Technology, Pasadena, California 91125, USA*

³*Division of Physics, Mathematics and Astronomy,
California Institute of Technology, Pasadena, California 91125, USA*

⁴*Alliance for Quantum Technologies, California Institute of Technology, Pasadena, California 91125, USA*

(Dated: August 7, 2019)

Quantum memories for light are important components for future long distance quantum networks. We present on-chip quantum storage of telecommunication band light at the single photon level in an ensemble of erbium-167 ions in an yttrium orthosilicate photonic crystal nanobeam resonator. Storage times of up to 10 μs are demonstrated using an all-optical atomic frequency comb protocol in a dilution refrigerator under a magnetic field of 380 mT. We show this quantum storage platform to have high bandwidth, high fidelity, and multimode capacity, and we outline a path towards an efficient erbium-167 quantum memory for light.

Optical quantum memories can aid processes involving the transfer of quantum information via photons, with applications in long distance quantum communication and quantum information processing [1–5]. Rare-earth ions in crystals are a promising solid-state platform for optical quantum memories due to their long-lived optical and spin transitions that are highly coherent at cryogenic temperatures [6, 7]. Among rare-earth ions, only erbium has been shown to possess highly coherent optical transitions in the telecommunication C-band, which allows for integration of memory systems with low loss optical fibers and integrated silicon photonics [8].

Fixed delay quantum storage for less than 50 ns at telecommunication wavelengths has been demonstrated in erbium-doped fibers [9], and lithium niobate waveguides [10] at efficiencies approaching 1%. The protocol used in both cases, the atomic frequency comb (AFC), requires spectrally selective optical pumping [11]. The storage efficiencies in these works were limited in part by the lack of suitable long-lived shelving states in the erbium ions in these hosts. Moving to isotopically purified erbium-167 in a yttrium orthosilicate host (YSO) offers the prospect of long-lived shelving states in the form of hyperfine levels [12]. While optical storage has been realized in erbium-doped YSO [13–15], including efficiencies approaching 50% at storage times of 16 μs (revival of silenced echo protocol [15]), quantum storage has yet to be demonstrated in this material.

In this work, we demonstrate on-chip quantum storage of telecommunication light at the single photon level. We used a nanophotonic crystal cavity milled directly in $^{167}\text{Er}^{3+}$ doped YSO ($^{167}\text{Er}^{3+}:\text{YSO}$) to couple to an ensemble of erbium ions and realize quantum storage using

the AFC protocol [11]. The cavity increased the absorption of light by the ion ensemble, allowing on-chip implementation of the memory protocol [16]. By working in a dilution refrigerator and using permanent magnets to apply a field of 380 mT, we accessed a regime in which the ions have optical coherence times of $\sim 150 \mu\text{s}$ and long lived spin states to allow spectral tailoring. For a storage time of 165 ns we achieved an efficiency of 0.2%, with lower efficiencies for longer storage times, up to 10 μs . We demonstrated storage of multiple temporal modes and measured a high fidelity of storage, exceeding the classical limit. Lastly, we identified the limits on the storage efficiency and proposed avenues for overcoming them to achieve an efficient $^{167}\text{Er}^{3+}:\text{YSO}$ quantum memory for light.

Memories using spectral tailoring such as the AFC protocol require a long-lived level within the optical ground state manifold, where population can be shelved. Hyperfine levels in the optical ground state in $^{167}\text{Er}^{3+}:\text{YSO}$ have been shown to have long lifetimes at 1.4 K and a magnetic field of 7 T [12]. In general, these levels can be long-lived when the erbium electron spin is frozen, which occurs when $\hbar\omega_e \gg k_B T$, where ω_e is the electron Zeeman splitting [12]. In this work, we satisfied this inequality by using a moderate magnetic field of 380 mT parallel to the D_1 axis of the crystal ($\omega_e = 2\pi \times 80 \text{ GHz}$) and a nanobeam temperature of $\sim 400 \text{ mK}$ (see Appendix A). The hyperfine lifetime was measured to be 29 minutes in the bulk crystal under the same magnetic field and cooling conditions.

Figures 1a and 1b show the nanoresonator used in this experiment. A triangular nanobeam photonic crystal cavity [17] was milled in a YSO crystal doped with isotopically purified $^{167}\text{Er}^{3+}$ (92% purity) at a nominal concentration of 50 ppm. The nanobeam was 1.5 μm wide, and $\sim 20 \mu\text{m}$ long. The slots in the nanobeam created a photonic crystal bandgap, and the periodic pattern (lattice constant = 590 nm,

* Currently at: Institute of Molecular Engineering, University of Chicago, Chicago, Illinois 60637, USA

† Corresponding author: faraon@caltech.edu

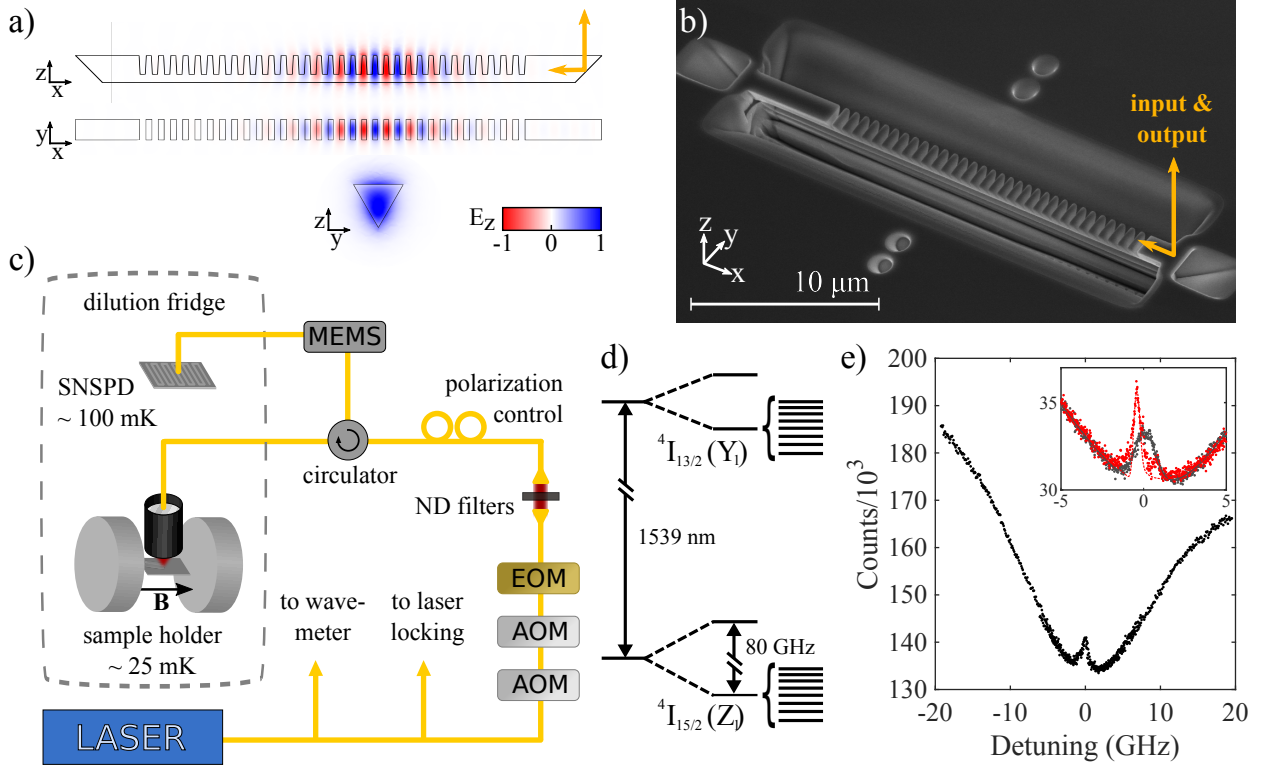


FIG. 1. (a) Finite element analysis simulation of the TM cavity mode in the triangular nanobeam resonator. Red-blue color gradient indicates the electric field component normal to the surface, E_z ; black outline indicates YSO-air interface; yellow arrow indicates coupling. (b) Scanning electron micrograph of the resonator, showing input/output coupling through a 45° angled slot coupler. (c) Schematic of experiment setup (details in main text). (d) Energy diagram of $^{167}\text{Er}^{3+}$:YSO, showing the $^4I_{15/2} \rightarrow ^4I_{13/2}$ optical transition for crystallographic site 2. (e) Reflection spectrum of cavity when tuned on resonance to the 1539 nm $^{167}\text{Er}^{3+}$:YSO transition. Detuning is measured from $194816 \text{ GHz} \pm 2 \text{ GHz}$. Inset shows a close-up of ion coupling before (black) and after (red) partial hyperfine initialization. Circles are data points; solid black and dashed red lines are fits to theory (see main text for details).

groove width = 450 nm) was modified quadratically in the center to create a cavity mode.

Figure 1c shows a schematic of the optical testing setup. A fiber-coupled tunable external-cavity diode laser was used to probe the nanobeam device and implement the AFC storage protocol. One percent of the laser light was directed to a wavemeter for measurement. Another $\sim 1\%$ of the light was picked off and sent to a locking setup, in which the laser frequency was stabilized by locking to a home-built fiber cavity using the Pound-Drever-Hall technique [18]. The remaining light was directed to the sample through two acousto-optical modulators (AOMs) for pulse shaping, as well as an electro-optic phase modulator (EOM) to control the phase of the light and to add strong sidebands for hyperfine initialization. Neutral density (ND) filters and polarization paddles provided attenuation and polarization control, respectively. A circulator directed light to the $^{167}\text{Er}^{3+}$:YSO crystal located inside a dilution refrigerator, thermally linked to the 25 mK stage. An aspheric lens pair focused light from an optical fiber onto the angled coupler of the resonator. A stack of xyz nanopositioners was used to optimize free space cou-

pling. Light from the resonator was directed by the circulator onto a superconducting nanowire single photon detector (SNSPD) at $\sim 100 \text{ mK}$. Strong initialization pulses were prevented from reaching the SNSPD by a micro electro-mechanical switch (MEMS). A magnetic field $\mathbf{B} = 380 \text{ mT}$ was applied to the sample using two cylindrical permanent magnets.

Figure 1d shows an energy diagram of an $^{167}\text{Er}^{3+}$ ion in YSO. Both ground and excited state manifolds have 16 hyperfine states ($I = 7/2$ nuclear spin, $S = 1/2$ effective electron spin), split into two sets of 8 by electron Zeeman coupling to the applied magnetic field. The optical transition used in this work couples the lower 8 hyperfine levels of the ground and excited state manifolds. The coherence time of this optical transition was measured using the two pulse photon echo method [19] to be $149 \mu\text{s} \pm 4 \mu\text{s}$ in the nanobeam. This provides an upper bound on all-optical storage time. In the bulk crystal, the optical coherence time of this transition under similar cooling conditions was measured to be $759 \mu\text{s} \pm 41 \mu\text{s}$. The reduction in coherence time as measured in the nanobeam is likely caused by a combination of higher temperature in the nanobeam during measurement and the impact of the

fabrication process. At 1 K, the coherence time of ions in the bulk crystal was found to be $136 \mu\text{s} \pm 9 \mu\text{s}$. In similar nanobeam devices [20, 21], focused ion beam milling has not significantly impacted the coherence properties of ions. However, the longer bulk coherence times measured in the current work allow a much more sensitive probe of the ions' environment. The optical coherence time did not limit the storage time achieved in this work.

Figure 1e shows the reflection spectrum of the nanobeam cavity, which has a measured loaded quality factor of 7×10^3 . The cavity was tuned onto resonance with the 1539 nm transition of the $^{167}\text{Er}^{3+}$ ions by freezing nitrogen gas onto the nanobeam at cryogenic temperatures [22]. The coupling of the ensemble of ions to the cavity is seen as a peak in the cavity reflection dip. The inset shows a close-up of the ion-cavity coupling (in black). The ensemble cooperativity was estimated from a fit to this curve to be 0.1 (see Appendix B).

For high efficiency storage using ions coupled to a cavity, the ensemble cooperativity should equal one [16, 23]. An increased ensemble cooperativity of 0.3 (inset of Fig. 1e, in red), was obtained using a partial hyperfine initialization procedure. The width of the 1539 nm transition in $^{167}\text{Er}^{3+}:\text{YSO}$ is ~ 1.5 GHz. This is broader than the true inhomogeneous linewidth of ~ 150 MHz because of the numerous closely spaced optical transitions arising from hyperfine splitting in both ground and excited state manifolds (see Fig. 1d). Because the ion population is distributed among the hyperfine ground states, the optical depth in the center of the 1539 nm line is lower compared to an $I = 0$ isotope. Therefore, to increase the ensemble cooperativity, the ion population was first initialized into a small number of hyperfine ground states with optical transitions in the center of the inhomogeneous line. This was achieved by sweeping the laser frequency between 350 MHz and 820 MHz on both sides of the inhomogeneous line. At 7 T, the entire optical ground state population can be initialized into one hyperfine state with an efficiency of 95% by pumping on all $\Delta m = +1$ or all $\Delta m = -1$ transitions [12]. At 380 mT $\parallel D_1$, only a partial initialization can be performed because the $\Delta m = \pm 1$ transitions are not fully spectrally resolved from the $\Delta m = 0$ transitions. The partial initialization procedure can be improved by using larger magnetic fields, or changing the angle of the applied field.

The nanobeam device was used to demonstrate quantum optical storage using the AFC protocol [11]. In this protocol, a pulse of light that is absorbed by an atomic frequency comb with an inter-tooth spacing of Δ is stored for $t = 1/\Delta$. Frequency selective optical pumping was used to create a comb within the inhomogeneous linewidth, as shown in Fig. 2a. Figure 2b shows a schematic of the protocol. First, a long pulse with strong frequency modulated sidebands was used for partial hyperfine initialization. The next 15 pulses, repeated $n_{\text{pump}} = 20$ times, created the comb: the laser frequency was swept through 15 values, separated by $\Delta = 6.1$ MHz,

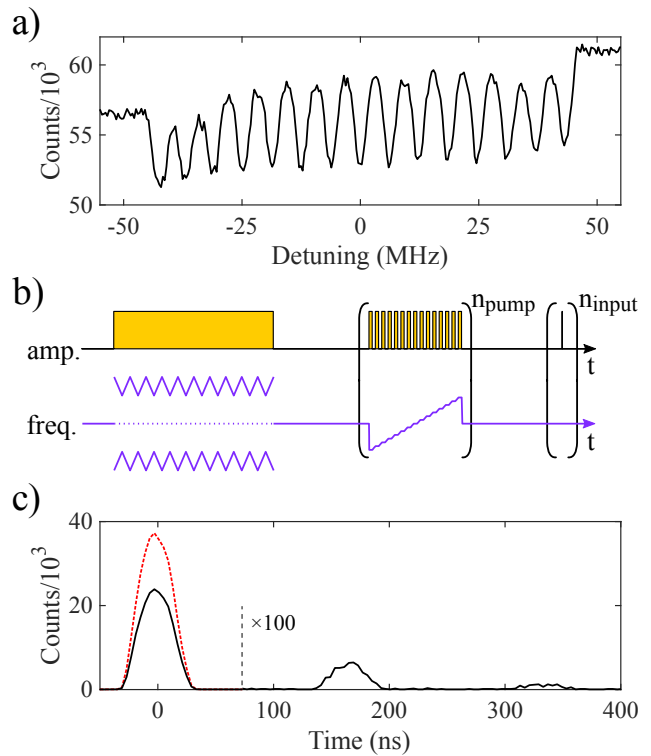


FIG. 2. (Color online) AFC experiment in the nanobeam cavity. (a) A section of the resonator reflection spectrum, showing an atomic frequency comb in the center of the inhomogeneously broadened $^{167}\text{Er}^{3+}$ transition. Detuning is measured from $194814.2 \text{ GHz} \pm 0.1 \text{ GHz}$. The apparent slope of the comb is due to its center frequency not being precisely aligned to the cavity resonance, leading to a dispersive shape. (b) Schematic of AFC pulse sequence showing amplitude (yellow) and frequency (purple) modulation of the laser (pulses not to scale, see main text for detail). (c) AFC storage: the input pulse (red dashed line) was partially absorbed by the comb; an output pulse was emitted at time $t = 1/\Delta = 165$ ns (black line, $\times 100$). The black line also shows the partially reflected input pulse ($t = 0$) and a smaller second output pulse at $t = 330$ ns.

to optically pump away ions and create 15 spectral transparencies. The following $n_{\text{input}} = 60$ pulses were zero-detuning weak coherent states which were stored in the frequency comb. The full experiment was repeated $\sim 10^4$ times. As shown in Fig. 2c, 60 ns wide pulses with an average photon number of $\bar{n} = 0.60 \pm 0.09$ were stored for 165 ns with an efficiency of 0.2%. Despite the partial initialization, the storage efficiency was limited by the ensemble cooperativity of the device (see Appendix D).

Coherent pulses could be stored in the device for up to $10 \mu\text{s}$, although with a lower efficiency of 10^{-5} , as shown in Fig. 3. Here, as for all storage times longer than 165 ns, we used an accumulated AFC method [24] to create the comb. As shown in the inset of Fig. 3, weak pairs of pulses separated by $t_{\text{storage}} = 10 \mu\text{s}$ were repeatedly sent into the cavity. The Fourier transform of each pulse pair is a frequency comb, which imprinted

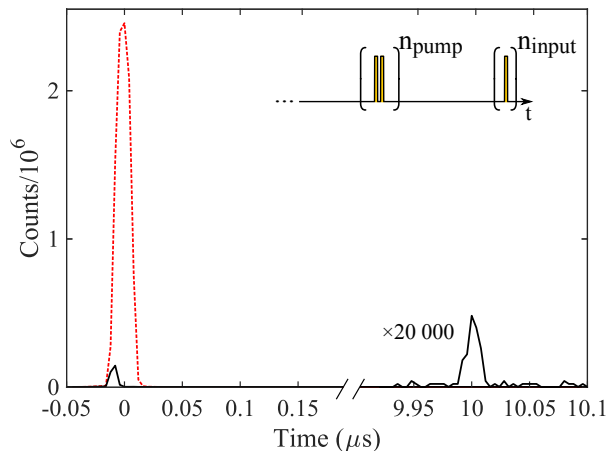


FIG. 3. (Color online) AFC storage for 10 μs in the nanobeam resonator. Red dashed line shows the input pulse. Black line shows the partially reflected input pulse and the output pulse ($\times 20\,000$). The reflected input pulse appears small due to detector saturation. Inset shows a schematic of the pulse sequence following hyperfine initialization. Pairs of comb preparation pulses 10 μs apart were repeated $n_{\text{pump}} = 10\,000$ times, followed by input pulses 20 ns wide, repeated $n_{\text{input}} = 10$ times.

onto the $^{167}\text{Er}^{3+}$ inhomogeneous line to create the AFC. This procedure utilized laser frequency stabilization during comb creation, which enabled the creation of fine-toothed AFCs required for longer storage. For the 165 ns storage, where a coarser AFC is practical, the procedure shown in Fig. 2b with no laser frequency stabilization led to higher efficiencies by creating a more consistent comb over the entire bandwidth. This is because the accumulated AFC has a sinc function envelope. The storage efficiency at 10 μs was limited by residual laser frequency jitter and by superhyperfine coupling to the yttrium ions in YSO. Superhyperfine coupling limits the narrowest spectral feature to ~ 1 MHz [25, 26]. Since this exceeds the period of the comb needed for this storage time ($\Delta = 1/t_{\text{storage}} = 0.1$ MHz), the resulting AFC will have a lower contrast, leading to lower storage efficiency.

The AFC protocol is capable of storing multiple temporal modes [11]. Ten coherent pulses were stored in this device, as shown in Fig. 4a. The AFC comb in Figure 2a has a bandwidth of ~ 90 MHz (see Fig. 2a) which can accommodate storage in multiple frequency modes [27]. An inhomogeneous linewidth of 150 MHz limits the bandwidth of storage in this system. Although there exist methods to increase this linewidth [28], the bandwidth cannot be increased much further before being limited by overlapping optical transitions from other hyperfine levels.

In quantum storage protocols, the phase of the stored state must be preserved. A double AFC was used as an interferometer in order to characterize the coherence of the storage process [24]. Two overlapping AFCs with

tooth spacing Δ_1, Δ_2 and with frequency detuning δ_1, δ_2 , were created, so that each input pulse was mapped to two output pulses at times $1/\Delta_1, 1/\Delta_2$ and with a relative phase $\phi_{\text{rel}} = 2\pi \left(\frac{\delta_2}{\Delta_2} - \frac{\delta_1}{\Delta_1} \right)$ [11]. An input state encoded into two pulses, $|\psi_{\text{in}}\rangle = \frac{1}{\sqrt{2}}(|\text{early}\rangle + |\text{late}\rangle)$, was therefore mapped to a total of four output pulses. By appropriately selecting the time interval between the early and late input pulses, two of the four output pulses were made to overlap and either constructively or destructively interfere, depending on ϕ_{rel} (see inset of Fig. 4b). Using an input state with mean photon number $\bar{n} = 0.6 \pm 0.09$, and sweeping ϕ_{rel} via the detuning δ_2 , the interference fringe shown in Fig. 4b was obtained (see caption for details). The measured visibility of $91.2\% \pm 3.4\%$ demonstrates the high degree of coherence of this on-chip storage process. The visibility was limited by the 12 counts in the total destructive interference case ($\delta_2 = \frac{\Delta_2}{2} \rightarrow \phi_{\text{rel}} = \pi$). These were due in part to imperfect cancellation of the two overlapping output pulses, resulting from the slightly different efficiencies of storage in the two AFCs, and in

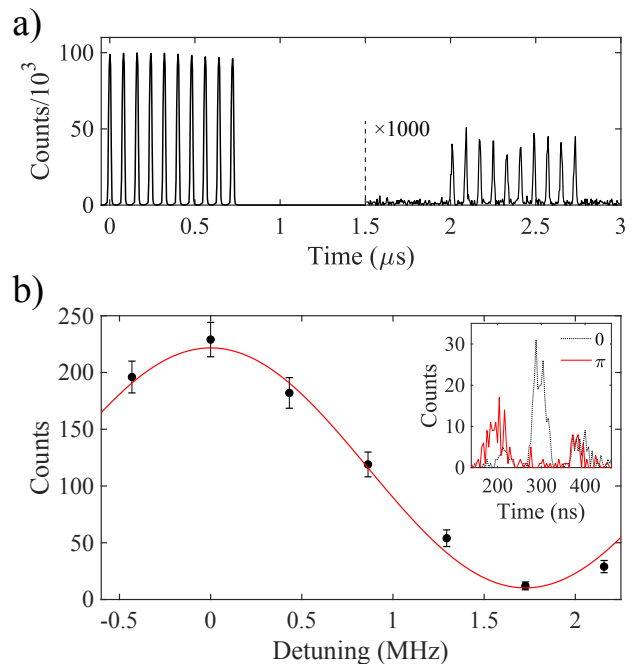


FIG. 4. (Color online) Multimode and coherent storage in the nanobeam resonator. (a) Storage of multiple temporal modes: ten 20 ns wide input pulses (reflection off cavity shown) and the corresponding 10 output pulses ($\times 1000$) from a 500 kHz AFC. (b) Visibility curve acquired using double comb experiment, with $\Delta_1 = 5.2$ MHz, $\Delta_2 = 3.4$ MHz, $\delta_1 = 0$ MHz. The detuning of the second comb was swept from $\delta_2 = -0.2$ MHz to $\delta_2 = 2.2$ MHz, and the intensity of the two central overlapping output pulses was measured. Black circles show the sum of counts in the overlapping pulse region with $\sqrt{N_{\text{counts}}}$ uncertainty bars. Red line shows a least squares fit to a sinusoid. Inset shows the four output pulses (middle two overlapping) in the case of the maximally constructive (dashed black line) and maximally destructive (solid red line) interference.

part to a dark count rate of 18.5 Hz, leading to a baseline of 7 counts. The dark-count-subtracted visibility is $97.0\% \pm 3.6\%$.

The double comb method was also used to estimate a lower bound for the fidelity of storing single photon time bin states, $F^{(n=1)}$. The fidelity of storage was measured for four input states $|\text{early}\rangle$, $|\text{late}\rangle$, $\frac{|\text{early}\rangle+|\text{late}\rangle}{\sqrt{2}}$ and $\frac{|\text{early}\rangle-|\text{late}\rangle}{\sqrt{2}}$, using two mean photon numbers $\bar{n} = 0.30$ and $\bar{n} = 0.60$. With these values, the decoy state method [27, 29] was used to calculate a bound on the fidelity for storing single photon states $F^{(n=1)} \geq 93.7\% \pm 2.4\%$, which exceeds the classical limit of $F = 2/3$ (details in Appendix C). Similar to the visibility case discussed above, the measured fidelity was limited in part by dark counts and in part by the double comb protocol being an imperfect interferometer. The dark counts limited fidelity bound was estimated to be $\sim 96.5\%$. Although the pulses stored in this experiment were weak coherent pulses, single [30–35] and entangled photon [36, 37] sources are available at telecommunication wavelengths, and storing photons of any frequency is enabled by quantum frequency conversion [38]. For efficient storage, the bandwidth of compatible photons is bounded by the $\gtrsim 1$ MHz periodicity and the $\lesssim 100$ MHz bandwidth of the AFC.

While the storage presented here was limited in efficiency, a nanophotonic cavity coupled to $^{167}\text{Er}^{3+}$ ions in YSO promises to be an efficient quantum storage system. The main limitations to the storage efficiency in this work were a low ensemble cooperativity of 0.3 and loss from the optical nanobeam cavity. The cooperativity can be increased using higher $^{167}\text{Er}^{3+}$ doping and better hyperfine initialization, which would require increasing the applied magnetic field [12] or changing its angle. A higher intrinsic quality factor resonator would serve to both increase cooperativity and decrease cavity loss. For example, using a YSO crystal with 200 ppm $^{167}\text{Er}^{3+}$ doping, optimal hyperfine initialization, and a resonator with an intrinsic quality factor of 2×10^6 , the theoretical efficiency of the AFC quantum storage is 90% (see Appendix D for analysis). Mature silicon nanofabrication technology can be leveraged to achieve this goal by using a silicon resonator evanescently coupled to $^{167}\text{Er}^{3+}$ ions in YSO [8, 33]. With this efficiency level and a storage time of $10\mu\text{s}$, the device would outperform a delay line composed of standard telecommunication fiber [39], an important benchmark on the way to achieving a quantum memory suitable for scalable quantum networks.

With the optical AFC protocol alone, it will be difficult to achieve efficient storage for this duration due to superhyperfine coupling. However, the AFC spin-wave protocol, where the stored information is reversibly transferred from the optical to the hyperfine manifold [11], would enable storage longer than $10\mu\text{s}$ without the same requirements for narrow spectral features, as well as enabling on-demand recall. The availability of hyperfine states with coherence times exceeding 1 second [12] make

$^{167}\text{Er}^{3+}:\text{YSO}$ a promising system for spin-wave storage.

In conclusion, we have demonstrated on-chip quantum storage of telecommunication band light at the single photon level. The storage had a bandwidth of ~ 90 MHz, and a storage fidelity for single photon states of at least $93.7\% \pm 2.4\%$. $^{167}\text{Er}^{3+}:\text{YSO}$ at temperatures of ~ 400 mK and moderate magnetic field was shown to be a promising material for AFC quantum memories. A clear path exists for creating a high efficiency quantum memory using this material and a nanoscale resonator.

ACKNOWLEDGMENTS

This work was supported by AFOSR Young Investigator Award [FA9550-15-1-0252], AFOSR Grant [FA9550-18-1-0374], and the National Science Foundation [EFRI 1741707]. I.C and J.R. acknowledge the support from the Natural Sciences and Engineering Research Council of Canada (NSERC) [PGSD2-502755-2017, PGSD3-502844-2017]. J.G.B. acknowledges the support of the American Australian Association’s Northrop Grumman Fellowship. N.S. acknowledges funding by the Alliance for Quantum Technologies’ Intelligent Quantum Networks and Technologies (INQNET) research program.

Appendix A: Device temperature

Due to poor thermal conduction at low temperatures in insulating materials such as YSO, and the small cross section of the nanobeam, the device was warmer than its ~ 25 mK surroundings when optical pulses were coupled in. The device temperature was estimated via the $^{167}\text{Er}^{3+}$ electron spin temperature [40], which was computed from the ratio between the lower and upper electron spin populations in the optical ground manifold using $\frac{N_{|\uparrow\rangle}}{N_{|\downarrow\rangle}} = e^{-\frac{\hbar\omega}{k_B T}}$.

Under an applied field of 380 mT, the electron spin in the optical ground state was frozen for any temperature under ~ 500 mK, enabling the long hyperfine lifetimes required for AFC storage. To be sensitive to lower temperatures, the electron spin population measurements were performed with a lower magnetic field of 110 mT (parallel to the D_1 axis of the crystal), leading to an electron Zeeman splitting of $\omega = 2\pi \times 23$ GHz, where the upper electron spin state had detectable population down to ~ 250 mK. Because the Zeeman splitting was still considerably greater than the hyperfine splitting, one can consider two electron spin states, $|\downarrow\rangle$ and $|\uparrow\rangle$, each split into eight by the hyperfine interaction. The population in the two electron spin states was measured via the electron-spin-preserving optical transitions from each level. The nanobeam was tuned such that these transitions were both resonant with the cavity, and photoluminescence (PL) was collected as a function of frequency, as shown in Fig. 5a. $N_{|\uparrow\rangle}/N_{|\downarrow\rangle}$ was extracted from the

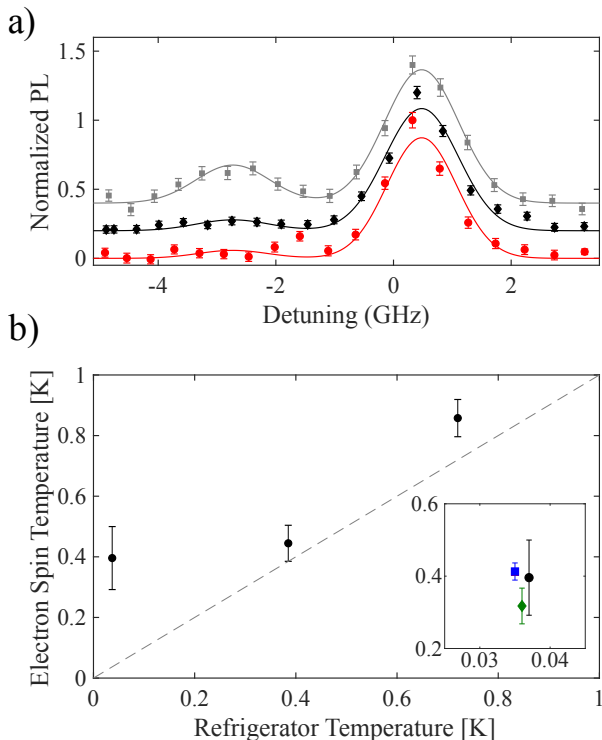


FIG. 5. a) Photoluminescence (PL) from the nanobeam device as a function of detuning at three refrigerator temperatures: 720 mK (gray squares), 385 mK (black diamonds), 37 mK (red circles). Detuning was measured from 194810 ± 0.1 GHz. PL was collected after a $500 \mu\text{s}$ resonant pulse at 0.3 pW (estimated power in nanobeam). Background counts were subtracted, and each curve was normalized and offset for clarity. Solid lines are fits to a sum of two Gaussians with equal widths and center frequencies 3.2 GHz apart. The $|\downarrow\rangle$ transition is at the higher frequency. b) Electron spin temperatures (EST) computed from the PL data in (a), as a function of refrigerator temperature. Dashed gray line indicates where the two temperatures are equal. The inset shows a closeup of the EST measurement at 37 mK (black circle) and the EST estimated during the T_2 measurement (green diamond) and the 165 ns storage experiment (blue square). To estimate the latter two temperatures, the same pattern of laser pulses as in the actual experiments was sent to the nanobeam, at 0.3 nW and 0.02 nW , respectively, and PL was collected after the pulses. Error bars are propagated standard deviations from photon counting ($\sqrt{N_{\text{counts}}}$). In all measurements the laser frequency was slowly modulated within each transition to prevent hyperfine holeburning.

area ratio of the two transitions. Figure 5b shows the electron spin temperatures computed from these ratios for different dilution refrigerator temperatures. The inset in Fig. 5b shows the electron spin temperature measured under input power conditions identical to two experiments: $317 \text{ mK} \pm 49 \text{ mK}$ for the T_2 measurement in the nanobeam and $413 \text{ mK} \pm 24 \text{ mK}$ for the 165 ns storage experiment in Fig. 2. Assuming the electron spin was in thermal equilibrium with the device, we therefore estimated the temperature of our device during experiments

to be $\sim 400 \text{ mK}$.

Appendix B: Ensemble cooperativity

To extract the cooperativity of coupling between the nanobeam resonator and the ensemble of $^{167}\text{Er}^{3+}$ ions, each cavity reflection spectrum shown in the inset of Fig. 1e was fit using

$$R = \alpha_1 \left| (1 - \alpha_f) + \alpha_f e^{i\theta_f} - \frac{i\kappa_{\text{in}}}{\omega - \omega_{\text{cavity}} + i\frac{\kappa}{2} + W(\omega, g_{\text{total}}, \Delta_{\text{ions}}, \omega_{\text{ions}})} \right|^2 + \alpha_2, \quad (\text{B1})$$

where $\alpha_{1,2}$ are amplitude and background fit parameters, $\alpha_f e^{i\theta_f}$ accounts for Fano interference (both α_f and θ_f are fit parameters), κ is the total cavity energy decay rate, κ_{in} is the coupling rate through the input/output port, and ω_{cavity} is the cavity resonance frequency. $\kappa = 27.3 \text{ GHz}$ and $\frac{\kappa_{\text{in}}}{\kappa} = 0.21$ were measured from reflectivity curves where the cavity was detuned from the $^{167}\text{Er}^{3+}$ transition. $W(\omega, g_{\text{total}}, \Delta_{\text{ions}}, \omega_{\text{ions}})$ is the absorption rate of the cavity field by the ensemble of ions, $W \sim \sum_i \frac{g_i^2}{\omega - \omega_i}$, where g_i is the coupling between one ion and the cavity [16, 41]. We approximated the irregular shape of the inhomogeneously and hyperfine broadened optical transition as a Gaussian, and used the expression for W from Reference [41]:

$$W = i \frac{\sqrt{\pi \log 2} g_{\text{total}}^2}{\Delta_{\text{ions}}/2} \left[1 - \text{erfz} \left(-\frac{i\sqrt{\log 2}(\omega - \omega_{\text{ions}})}{\Delta_{\text{ions}}/2} \right) \right] \times \exp \left[-\sqrt{\log 2} \left(\frac{\omega - \omega_{\text{ions}}}{\Delta_{\text{ions}}/2} \right)^2 \right], \quad (\text{B2})$$

where Δ_{ions} is the linewidth of the ensemble transition, ω_{ions} its the center, and $g_{\text{total}}^2 = \sum_i g_i^2$. Finally, the ensemble cooperativity was computed using $C = \frac{|W(\omega=\omega_{\text{ions}})|}{\kappa/2} = \frac{4\sqrt{\pi \log 2} g_{\text{total}}^2}{\kappa \Delta_{\text{ions}}} [8]$.

For the case with no initialization, the fit yielded: $\omega_{\text{cavity}} - \omega_{\text{ions}} = 2\pi \times 2.5 \text{ GHz}$, $g_{\text{total}} = 2\pi \times 0.79 \text{ GHz}$, $\Delta_{\text{ions}} = 2\pi \times 1.4 \text{ GHz}$, $C = 0.1$.

For the case with initialization, the fit yielded: $\omega_{\text{cavity}} - \omega_{\text{ions}} = 2\pi \times 1.5 \text{ GHz}$, $g_{\text{total}} = 2\pi \times 0.70 \text{ GHz}$, $\Delta_{\text{ions}} = 2\pi \times 0.36 \text{ GHz}$, $C = 0.3$.

Appendix C: Fidelity

In the absence of a single photon source, a lower bound on the storage fidelity of a single photon input state can be found using the decoy state analysis method [27, 29]. In this method, a time bin state ψ with a mean photon number \bar{n} is stored using the AFC protocol, and the

fidelity $F_\psi^{(\bar{n})}$ of storage is measured as

$$F_\psi^{(\bar{n})} = \frac{N_\psi}{N_\psi + N_{\phi \perp \psi}}, \quad (\text{C1})$$

where N_ψ ($N_{\phi \perp \psi}$) is the number of photons measured in the output time bin corresponding to ψ ($\phi \perp \psi$), and $\phi \perp \psi$ denotes the state orthogonal to ψ . The gain of the output, $Q_\psi^{(\bar{n})}$ is also estimated using,

$$Q_\psi^{(\bar{n})} = N_\psi + N_{\phi \perp \psi}. \quad (\text{C2})$$

$F_\psi^{(\bar{n})}$ and $Q_\psi^{(\bar{n})}$ are measured for mean photon numbers \bar{n}_1 and \bar{n}_2 , where $\bar{n}_1 < \bar{n}_2$, and $\bar{n}_2 < 1$.

The lower bound on the fidelity of storing a one-photon input state $F_\psi^{(n=1,L)}$ is then computed using:

$$F_\psi^{(n=1,L)} = 1 - \frac{E_\psi^{(\bar{n}_1)} Q^{(\bar{n}_1)} \exp \bar{n}_1 - E^{(0)} Y^{(0)}}{Y^{(n=1,L)} \bar{n}_1}, \quad (\text{C3})$$

where

$$E_\psi^{(\bar{n})} = 1 - F_\psi^{(\bar{n})} \quad (\text{C4})$$

is the error rate of storing a state ψ with mean photon number \bar{n} , and

$$Y^{(n=1,L)} = \max \left\{ Y^{(0)}, \frac{\bar{n}_2}{\bar{n}_2 \bar{n}_1 - \bar{n}_1^2} \left(Q^{(\bar{n}_1)} e^{\bar{n}_1} - Q^{(\bar{n}_2)} e^{\bar{n}_2} \frac{\bar{n}_1^2}{\bar{n}_2^2} - \frac{\bar{n}_2^2 - \bar{n}_1^2}{\bar{n}_2^2} Y^{(0)} \right) \right\} \quad (\text{C5})$$

is the lower bound on the detection yield for the storage of a single photon state (see Reference [29]). $Y^{(0)} = Q^{(n=0)}$ is the yield when the input state is vacuum, equal to the dark counts in both output time bins. The superscripts denote photon number, and whether the value is a lower bound (L). $E^{(0)} = E^{(n=0)}$ is the vacuum error rate, which is 0.5 by definition [29].

In order to obtain an average fidelity bound for all possible time bin states, the fidelities for storing time bin states $|\text{early}\rangle$, $|\text{late}\rangle$, $|+\rangle = \frac{|\text{early}\rangle + |\text{late}\rangle}{\sqrt{2}}$ and $|-\rangle = \frac{|\text{early}\rangle - |\text{late}\rangle}{\sqrt{2}}$ were measured for input photon numbers $\bar{n} = 0.30$ and $\bar{n} = 0.60$. The input pulses defining the $|\text{early}\rangle$ and $|\text{late}\rangle$ basis were 60 ns wide and 90 ns apart. A double AFC was used for measurements of all states, with the memory times associated with the two combs being $t_1 = 210$ ns and $t_2 = 300$ ns, such that $t_2 - t_1 = 90$ ns. Of the three output time bins (see inset of Fig. 4b), the first and third were used for measuring F_{early} and F_{late} while the second time bin was used for measuring F_+ and F_- .

Following Equation C3, $F_+^{(n=1,L)}$ was computed using:

$$F_+^{(n=1,L)} = 1 - \frac{E_+^{(\bar{n}_1)} Q_{+/-}^{(\bar{n}_1)} \exp \bar{n}_1 - E^{(0)} Y_{+/-}^{(0)}}{Y_{+/-}^{(n=1,L)} \bar{n}_1}, \quad (\text{C6})$$

with similar equations for the other three states. $Q_{+/-}^{(\bar{n}_1)}$, $Y_{+/-}^{(0)}$, and $Y_{+/-}^{(n=1,L)}$ are averaged over the $|+\rangle$ and $|-\rangle$ fidelity measurements.

The lower bound on the fidelity of storing an arbitrary single photon state, $F_{\text{average}}^{(n=1,L)} = 93.7\% \pm 2.4\%$, was then computed as follows:

$$F_{\text{average}}^{(n=1,L)} = \frac{1}{3} \left(\frac{F_{\text{early}}^{(n=1,L)} + F_{\text{late}}^{(n=1,L)}}{2} \right) + \frac{2}{3} \left(\frac{F_+^{(n=1,L)} + F_-^{(n=1,L)}}{2} \right). \quad (\text{C7})$$

Table I summarizes the measured fidelity values for storing weak coherent states. The uncertainties are calculated based on $\sqrt{N_{\text{photon}}}$ standard deviation on all N_ψ values due to Poissonian statistics of photon counting and the uncertainty, estimated to be 15%, of the mean input photon numbers, \bar{n} .

Input photon number	$\frac{1}{2} (F_{\text{early}}^{(\bar{n})} + F_{\text{late}}^{(\bar{n})})$	$\frac{1}{2} (F_+^{(\bar{n})} + F_-^{(\bar{n})})$
$\bar{n} = 0.60 \pm 0.09$	$89.04\% \pm 1.34\%$	$91.90\% \pm 1.32\%$
$\bar{n} = 0.30 \pm 0.05$	$82.59\% \pm 1.80\%$	$90.75\% \pm 1.84\%$
$n = 0$	50%	50%

TABLE I. Measured storage fidelities in the nanobeam device.

Appendix D: Storage efficiency

The efficiency of AFC storage in a cavity is given by [16, 21, 23]:

$$\eta_{\text{AFC}} = \left(\frac{4\kappa_{\text{in}} \Gamma_{\text{comb}}}{(\kappa_{\text{total}} + \Gamma_{\text{comb}} + \Gamma_{\text{bg}})^2} \right)^2 \eta_d, \quad (\text{D1})$$

where κ_{in} is the rate of cavity coupling through the input/output port, κ_{total} is the total energy decay rate of the cavity, $\eta_d = \exp\left(-\frac{\pi^2}{2 \ln 2 (\Delta/\gamma)^2}\right)$ accounts for dephasing due to the finite width of comb teeth [11], and Γ_{comb} and Γ_{bg} are the absorption rates of the cavity field by the ensemble of ions in the comb and background, respectively. Background ions are those ions remaining after optical pumping, with transition frequencies where transparency is desired (i.e. between the teeth of the comb). Nonzero Γ_{bg} results from limitations in spectral holeburning. Using η_{spectral} , the fractional optical depth of a spectral hole, Δ , the inter-tooth spacing, and γ , the width of one comb tooth, these can be estimated as follows:

$$\Gamma_{\text{comb}} \approx \eta_{\text{spectral}} \frac{\gamma}{\Delta} \Gamma_{\text{ions}}, \quad (\text{D2})$$

$$\Gamma_{\text{bg}} = (1 - \eta_{\text{spectral}}) \Gamma_{\text{ions}}, \quad (\text{D3})$$

where $\Gamma_{\text{ions}} = |W(\omega = \omega_{\text{ions}})| = \frac{\sqrt{\pi \log 2} g_{\text{total}}^2}{\Delta_{\text{ions}}/2}$ is the absorption rate of the cavity field by the ensemble of ions before comb preparation (see Appendix B).

We can define an effective AFC cooperativity, C' :

$$C' = \frac{\Gamma_{\text{comb}} + \Gamma_{\text{bg}}}{\kappa_{\text{total}}/2} = (\eta_{\text{spectral}} \frac{\gamma}{\Delta} + (1 - \eta_{\text{spectral}})) C. \quad (\text{D4})$$

Rewriting Equation D1 gives rise to the following expression for the AFC storage efficiency:

$$\eta_{\text{AFC}} = \left(\frac{1}{\frac{\Delta}{\gamma} \left(\frac{1}{\eta_{\text{spectral}}} - 1 \right) + 1} \frac{\kappa_{\text{in}}}{\kappa_{\text{total}}} \frac{4C'}{(1 + C')^2} \right)^2 \eta_d, \quad (\text{D5})$$

The efficiency is maximized when $C' \rightarrow 1$.

The predicted efficiency of storage in the nanobeam is $\eta_{\text{AFC}} = 0.17\%$, found using $C = 0.3$, $\frac{\kappa_{\text{in}}}{\kappa_{\text{total}}} = 0.21$, a measured finesse of $\Delta/\gamma = 2.1$, and by assuming a perfect comb, $\eta_{\text{spectral}} = 1$. This is similar to the measured value of 0.20% for a storage time of 165 ns.

To improve the memory efficiency, the ensemble cooperativity and the ratio $\frac{\kappa_{\text{in}}}{\kappa_{\text{total}}}$ must be increased. We first consider improvements to the concentration and initialization of $^{167}\text{Er}^{3+}$ ions, keeping the nanophotonic resonator the same. By increasing the ion concentration to 200 ppm (assuming no significant increase in inhomogeneous linewidth), and using the level of initialization achieved in Reference [12] (95%), a cooperativity of $C = 3$ is expected. Using the measured $\frac{\kappa_{\text{in}}}{\kappa_{\text{total}}} = 0.21$, and a comb

finesse of $\Delta/\gamma = 3$, ($C' = 0.73$), the predicted efficiency is 3%. This memory efficiency is mainly limited by the loss from the cavity, term $\left(\frac{\kappa_{\text{in}}}{\kappa_{\text{total}}} \right)^2$ in equation D5. The total cavity loss rate is $\kappa_{\text{total}} = \kappa_{\text{in}} + \kappa_i$, where κ_i is the intrinsic loss, including losses from absorption, scattering and the imperfect reflectivity of the second mirror.

A memory efficiency greater than 90% can be achieved if the intrinsic quality factor of the resonator is increased from its current value of $Q_i \sim 9000$ to 2×10^6 , while increasing $\frac{\kappa_{\text{in}}}{\kappa_{\text{total}}}$ to 0.97. The latter can be accomplished using a resonator with one mirror having a relatively low reflectivity, and with minimal losses through other channels (transmission through second mirror, scattering, absorption). This calculation assumes the same material as described above (200 ppm, ideal initialization into one hyperfine state), and a comb finesse of ~ 13 . It also accounts for a decrease by a factor of ~ 3 in the cooperativity that results from switching to a hybrid silicon-YSO platform where the evanescent cavity-ion coupling is weaker. With this storage efficiency, the memory would match the performance of an optical fiber (0.15 dB/km) at $t_{\text{storage}} = 10 \mu\text{s}$ [39].

For a finesse of 13 and a storage time of 10 μs , the corresponding comb tooth width is $\gamma = \frac{\Delta}{\text{finesse}} = 8 \text{ kHz}$, which is too narrow for $^{167}\text{Er}^{3+}$:YSO, where effective linewidths are limited to 1 MHz by superhyperfine coupling. However, memory times longer than 10 μs can be achieved with a nanoresonator in this material by using the spin-wave AFC [11].

-
- [1] H. J. Kimble, The quantum internet, *Nature* **453**, 1023 (2008).
- [2] K. Heshami, D. G. England, P. C. Humphreys, P. J. Bustard, V. M. Acosta, J. Nunn, and B. J. Sussman, Quantum memories: emerging applications and recent advances, *Journal of Modern Optics* **63**, 2005 (2016).
- [3] H.-J. Briegel, W. Dür, J. I. Cirac, and P. Zoller, Quantum repeaters: The role of imperfect local operations in quantum communication, *Phys. Rev. Lett.* **81**, 5932 (1998).
- [4] P. Kok, W. J. Munro, K. Nemoto, T. C. Ralph, J. P. Dowling, and G. J. Milburn, Linear optical quantum computing with photonic qubits, *Rev. Mod. Phys.* **79**, 135 (2007).
- [5] C. Monroe, R. Raussendorf, A. Ruthven, K. R. Brown, P. Maunz, L.-M. Duan, and J. Kim, Large-scale modular quantum-computer architecture with atomic memory and photonic interconnects, *Phys. Rev. A* **89**, 022317 (2014).
- [6] C. Thiel, T. Böttger, and R. Cone, Rare-earth-doped materials for applications in quantum information storage and signal processing, *Journal of Luminescence* **131**, 353 (2011).
- [7] M. Zhong, M. P. Hedges, R. L. Ahlefeldt, J. G. Bartholomew, S. E. Beavan, S. M. Wittig, J. J. Longdell, and M. J. Sellars, Optically addressable nuclear spins in a solid with a six-hour coherence time, *Nature* **517**, 177 (2015).
- [8] E. Miyazono, I. Craiciu, A. Arbabi, T. Zhong, and A. Faraon, Coupling erbium dopants in yttrium orthosilicate to silicon photonic resonators and waveguides, *Opt. Express* **25**, 2863 (2017).
- [9] E. Saglamyurek, J. Jin, V. B. Verma, M. D. Shaw, F. Marsili, S. W. Nam, D. Oblak, and W. Tittel, Quantum storage of entangled telecom-wavelength photons in an erbium-doped optical fibre, *Nature Photonics* **9**, 83 (2015).
- [10] M. F. Askarani, M. G. Puigibert, T. Lutz, V. B. Verma, M. D. Shaw, S. W. Nam, N. Sinclair, D. Oblak, and W. Tittel, Storage and reemission of heralded telecommunication-wavelength photons using a crystal waveguide, *Phys. Rev. Applied* **11**, 054056 (2019).
- [11] M. Afzelius, C. Simon, H. de Riedmatten, and N. Gisin, Multimode quantum memory based on atomic frequency combs, *Phys. Rev. A* **79**, 052329 (2009).
- [12] M. Rancić, M. P. Hedges, R. L. Ahlefeldt, and M. J. Sellars, Coherence time of over a second in a telecommunication-compatible quantum memory storage material, *Nature Physics* **14**, 50 (2018).
- [13] B. Lauritzen, J. Minář, H. de Riedmatten, M. Afzelius, N. Sangouard, C. Simon, and N. Gisin, Telecommunication-wavelength solid-state memory at

- the single photon level, *Phys. Rev. Lett.* **104**, 080502 (2010).
- [14] B. Lauritzen, J. Minář, H. de Riedmatten, M. Afzelius, and N. Gisin, Approaches for a quantum memory at telecommunication wavelengths, *Phys. Rev. A* **83**, 012318 (2011).
- [15] J. Dajczgewand, J.-L. L. Gouët, A. Louchet-Chauvet, and T. Chanelière, Large efficiency at telecom wavelength for optical quantum memories, *Opt. Lett.* **39**, 2711 (2014).
- [16] M. Afzelius and C. Simon, Impedance-matched cavity quantum memory, *Phys. Rev. A* **82**, 022310 (2010).
- [17] T. Zhong, J. Rochman, J. M. Kindem, E. Miyazono, and A. Faraon, High quality factor nanophotonic resonators in bulk rare-earth doped crystals, *Opt. Express* **24**, 536 (2016).
- [18] R. W. P. Drever, J. L. Hall, F. V. Kowalski, J. Hough, G. M. Ford, A. J. Munley, and H. Ward, Laser phase and frequency stabilization using an optical resonator, *Appl. Phys. B* **31**, 97 (1983).
- [19] I. D. Abella, N. A. Kurnit, and S. R. Hartmann, Photon echoes, *Phys. Rev.* **141**, 391 (1966).
- [20] T. Zhong, J. M. Kindem, E. Miyazono, and A. Faraon, Nanophotonic coherent light-matter interfaces based on rare-earth-doped crystals, *Nature Communications* **6**, 8206 (2015).
- [21] T. Zhong, J. M. Kindem, J. G. Bartholomew, J. Rochman, I. Craiciu, E. Miyazono, M. Bettinelli, E. Cavalli, V. Verma, S. W. Nam, F. Marsili, M. D. Shaw, A. D. Beyer, and A. Faraon, Nanophotonic rare-earth quantum memory with optically controlled retrieval, *Science* 10.1126/science.aan5959 (2017).
- [22] S. Mosor, J. Hendrickson, B. C. Richards, J. Sweet, G. Khitrova, H. M. Gibbs, T. Yoshie, A. Scherer, O. B. Shchekin, and D. G. Deppe, Scanning a photonic crystal slab nanocavity by condensation of xenon, *Applied Physics Letters* **87**, 141105 (2005).
- [23] S. A. Moiseev, S. N. Andrianov, and F. F. Gubaidullin, Efficient multimode quantum memory based on photon echo in an optimal qed cavity, *Phys. Rev. A* **82**, 022311 (2010).
- [24] H. de Riedmatten, M. Afzelius, M. U. Staudt, C. Simon, and N. Gisin, A solid-state light-matter interface at the single-photon level, *Nature* **456**, 773 (2008).
- [25] O. Guillot-Noël, H. Vezin, P. Goldner, F. Beaudoux, J. Vincent, J. Lejay, and I. Lorgeré, Direct observation of rare-earth-host interactions in Er : Y₂SiO₅, *Phys. Rev. B* **76**, 180408 (2007).
- [26] B. Car, L. Veissier, A. Louchet-Chauvet, J.-L. Le Gouët, and T. Chanelière, Selective optical addressing of nuclear spins through superhyperfine interaction in rare-earth doped solids, *Phys. Rev. Lett.* **120**, 197401 (2018).
- [27] N. Sinclair, E. Saglamyurek, H. Mallahzadeh, J. A. Slater, M. George, R. Ricken, M. P. Hedges, D. Oblak, C. Simon, W. Sohler, and W. Tittel, Spectral multiplexing for scalable quantum photonics using an atomic frequency comb quantum memory and feed-forward control, *Phys. Rev. Lett.* **113**, 053603 (2014).
- [28] S. Welinski, C. W. Thiel, J. Dajczgewand, A. Ferrier, R. L. Cone, R. M. Macfarlane, T. Chanelière, A. Louchet-Chauvet, and P. Goldner, Effects of disorder on optical and electron spin linewidths in Er³⁺, Sc³⁺:Y₂SiO₅, *Optical Materials* **63**, 69 (2017).
- [29] X. Ma, B. Qi, Y. Zhao, and H.-K. Lo, Practical decoy state for quantum key distribution, *Phys. Rev. A* **72**, 012326 (2005).
- [30] S. A. Zargaleh, S. Hameau, B. Eble, F. Margailan, H. J. von Bardeleben, J. L. Cantin, and W. Gao, Nitrogen vacancy center in cubic silicon carbide: A promising qubit in the 1.5 μm spectral range for photonic quantum networks, *Phys. Rev. B* **98**, 165203 (2018).
- [31] J. Wang, Y. Zhou, Z. Wang, A. Rasmita, J. Yang, X. Li, H. J. von Bardeleben, and W. Gao, Bright room temperature single photon source at telecom range in cubic silicon carbide, *Nature Communications* **9**, 4106 (2018).
- [32] D. Rieländer, A. Lenhard, M. Mazzer, and H. de Riedmatten, Cavity enhanced telecom heralded single photons for spin-wave solid state quantum memories, *New Journal of Physics* **18**, 123013 (2016).
- [33] A. M. Dibos, M. Raha, C. M. Phenicie, and J. D. Thompson, Atomic source of single photons in the telecom band, *Phys. Rev. Lett.* **120**, 243601 (2018).
- [34] M. Paul, F. Olbrich, J. Hschele, S. Schreier, J. Kettler, S. L. Portalupi, M. Jetter, and P. Michler, Single-photon emission at 1.55 μm from MOVPE-grown InAs quantum dots on InGaAs/GaAs metamorphic buffers, *Applied Physics Letters* **111**, 033102 (2017).
- [35] S. Atzeni, A. S. Rab, G. Corrielli, E. Polino, M. Valeri, P. Mataloni, N. Spagnolo, A. Crespi, F. Sciarrino, and R. Osellame, Integrated sources of entangled photons at the telecom wavelength in femtosecond-laser-written circuits, *Optica* **5**, 311 (2018).
- [36] K. Niizeki, K. Ikeda, M. Zheng, X. Xie, K. Okamura, N. Takei, N. Namekata, S. Inoue, H. Kosaka, and T. Horikiri, Ultrabright narrow-band telecom two-photon source for long-distance quantum communication, *Applied Physics Express* **11**, 042801 (2018).
- [37] Y. Zhou, Z. Wang, A. Rasmita, S. Kim, A. Berhane, Z. Bodrog, G. Adamo, A. Gali, I. Aharonovich, and W.-b. Gao, Room temperature solid-state quantum emitters in the telecom range, *Science Advances* **4**, 10.1126/sciadv.aar3580 (2018).
- [38] A. Dréau, A. Tchebotareva, A. E. Mahdaoui, C. Bonato, and R. Hanson, Quantum frequency conversion of single photons from a nitrogen-vacancy center in diamond to telecommunication wavelengths, *Phys. Rev. Applied* **9**, 064031 (2018).
- [39] Y.-W. Cho, G. T. Campbell, J. L. Everett, J. Bernu, D. B. Higginbottom, M. T. Cao, J. Geng, N. P. Robins, P. K. Lam, and B. C. Buchler, Highly efficient optical quantum memory with long coherence time in cold atoms, *Optica* **3**, 100 (2016).
- [40] N. Kukharchyk, D. Sholokhov, O. Morozov, S. L. Korabeleva, A. A. Kalachev, and P. A. Bushev, Optical coherence of ¹⁶⁶Er:⁷LiYF₄ crystal below 1 K, *New Journal of Physics* **20**, 023044 (2018).
- [41] I. Diniz, S. Portolan, R. Ferreira, J. M. Gérard, P. Bertet, and A. Auffèves, Strongly coupling a cavity to inhomogeneous ensembles of emitters: Potential for long-lived solid-state quantum memories, *Phys. Rev. A* **84**, 063810 (2011).